HHS Public Access

Author manuscript

Nature. Author manuscript; available in PMC 2014 November 08.

Published in final edited form as:

Nature. 2014 May 8; 509(7499): 183–188. doi:10.1038/nature13135.

FXR is a molecular target for the effects of vertical sleeve gastrectomy

Karen K. Ryan[1], **Valentina Tremaroli**[2], **Christoffer Clemmensen**[1,3], **Petia Kovatcheva-Datchary**[2], **Andriy Myronovych**[4], **Rebekah Karns**[5], **Hilary E. Wilson-Pérez**[1], **Darleen A. Sandoval**[1], **Rohit Kohli**[4], **Fredrik Bäckhed**[2,6], and **Randy J. Seeley**[1]

[1]Department of Internal Medicine, Division of Endocrinology, Diabetes and Metabolism, University of Cincinnati, Cincinnati, Ohio, USA

[2]Wallenberg Laboratory, Department of Molecular and Clinical Medicine and Sahlgrenska Center for Cardiovascular and Metabolic Research, University of Gothenburg, S-413 45 Gothenburg, Sweden

[3]Department of Drug Design and Pharmacology, Faculty of Health and Medical Sciences, University of Copenhagen, Universitetsparken 2, DK-2100 Copenhagen, Denmark

[4]Department of Pediatrics, Division of Gastroenterology, Hepatology, and Nutrition

[5]Divison of Biomedical Informatics Cincinnati Children's Hospital Medical Center, Cincinnati, Ohio, USA

[6]Novo Nordisk Foundation Center for Basic Metabolic Research, Section for Metabolic Receptology and Enteroendocrinology, Faculty of Health Sciences, University of Copenhagen, Copenhagen, DK-2200, Denmark.

SUMMARY

Bariatric surgical procedures, such as vertical sleeve gastrectomy (VSG), are currently the most effective therapy for the treatment of obesity, and are associated with substantial improvements in co-morbidities, including type-2 diabetes mellitus. The underlying molecular mechanisms contributing to these benefits remain largely undetermined, despite offering tremendous potential to reveal new targets for therapeutic intervention. The present study demonstrates that the therapeutic value of VSG does not result from mechanical restriction imposed by a smaller stomach. Rather, we report that VSG is associated with increased circulating bile acids, and associated changes to gut microbial communities. Moreover, in the absence of nuclear bile acid

Correspondence and requests for materials should be addressed to randy.seeley@uc.edu..

AUTHOR CONTRIBUTIONS

K.K.R. conceptualized, designed, performed and analyzed the experiments and wrote the manuscript. C.C., A.M., H.E. W-P, D.A.S. and R. Kohli performed experiments and edited the manuscript. R. Karns performed the bioinformatics analysis of the RNA-seq data. R.V.T. and F.B. designed and performed the microbiota analysis and edited the manuscript. P. K-D and F.B. designed and performed the analysis of cecal metabolites and edited the manuscript. R.J.S. conceptualized, designed and analyzed the experiments and wrote the manuscript.

The other authors have nothing to declare.

Detailed methods are provided in the Supplemental Information.

receptor FXR, the ability of VSG to reduce body weight and improve glucose tolerance is substantially reduced. These results point to bile acids and FXR signaling as an important molecular underpinning for the beneficial effects of this weight-loss surgery.

INTRODUCTION

Perhaps surprisingly, the most effective and durable therapies for the treatment of obesity involve surgical, rather than pharmacological or behavioral intervention. In contrast to the modest impact of diet and exercise, most individuals that lose weight with bariatric surgery maintain reduced levels of body fat for many years[1]. This is associated with substantial improvements in co-morbidities. Notably, 40% of obese T2DM patients that undergo bariatric surgery achieve full remission within one year[2]. Despite its efficacy, however, surgery is not an attractive therapeutic option for many individuals suffering from obesity and its consequences. Therefore it is both scientifically and clinically imperative that we identify molecular mechanisms responsible for weight loss and other metabolic improvements, to target affected pathways in a less-invasive manner.

Vertical Sleeve Gastrectomy (VSG) is a bariatric procedure in which approximately 80% of the stomach is removed along the greater curvature. This creates a gastric “sleeve” in continuity with the esophagus and duodenum. VSG induces loss of body weight and fat mass, and improves glucose tolerance in humans and in rodents[2,3]. Importantly the efficacy of VSG is comparable to the more complex Roux-en-y gastric bypass (RYGB), which not only creates a smaller stomach but also involves surgical re-routing of the small intestine[4,5]. A recent randomized controlled trial found that VSG and RYGB produced nearly the same T2DM remission after one year, and that both procedures were significantly superior to medical management[2].

Conventional wisdom holds that bariatric surgeries, including VSG and RYGB, lead to weight loss and resolution of T2DM directly as a result of reducing the ability of the stomach to physically accommodate a meal. That is, the stomach is made smaller, perhaps imposing a mechanical restriction on the amount of food that can be consumed at one time. Moreover, in RYGB, the flow of nutrients and biliopancreatic secretions is re-routed, perhaps limiting macronutrient absorption. However, growing evidence indicates that restriction and malabsorption are not the primary mechanisms driving weight loss and other metabolic improvements after bariatric surgery[6]. As just one example, a substantial proportion of diabetic patients are able to stop taking their medications within days of surgery, before substantial weight loss has occured[2]. Given the short time frame, some controversy exists about the mechanisms underlying this dramatic outcome. Some hypothesize that acute improvements are independent of weight loss and result from changes in gut physiology, including altered neurohumoral signaling or altered microbial ecology. In contrast, others suggest these benefits are the result of the hypocaloric post-operative mileui and rapid weight loss[7,8].

Among the changes to gut physiology that occurs following bariatric surgery, is altered enterohepatic circulation of bile acids. Both RYGB and VSG are associated with a substantial increase in circulating total bile acids in humans and in rodent models[9,10]. It is

now clear that, in addition to aiding the mechanical digestion and absorption of lipids, bile acids also bind to the nuclear receptor FXR (farnesoid-x receptor) to function as signaling molecules contributing to the regulation of various metabolic processes. In light of this role, we hypothesized that FXR-signaling links altered bile acid homeostasis to important post-operative changes in metabolism and gut microbial communities, thereby contributing to the maintenance of weight loss and improvements in glucose control observed following VSG. To test this hypothesis, we applied VSG surgery to diet-induced obese mice with targeted genetic disruption of FXR and their wild-type littermates.

RESULTS

Unbiased pathway analysis

We used mRNA-seq, together with subsequent unbiased pathway analysis, to identify key biological pathways that were altered in the distal small intestine following VSG (Fig 1). Consistent with our recent report that VSG significantly alters the expression of hepatic genes involved in lipid and bile acid metabolism[9], the pathway 'Nuclear receptors in lipid metabolism and toxicity' emerged as one of the top pathways enriched in genes differentially regulated (fold change >= 1.5) in VSG (p=7.18E-5). Intriguingly, among the other top pathways, several point towards an altered gut microbiota. Specifically, the glutathione pathway (p=6.00E-8), which plays important roles in nutrient metabolism and antioxidant defense, is known to be significantly altered by the presence/absence of a microbiota—and this is associated with changes in bile acid composition[11,12]. Likewise, many of the biotransformations (p=4.81E-5) that are increased likely reflect an altered microbiota, induced for detoxification of metabolites such as secondary bile acids. Finally, changes in gut microbial communities have been extensively linked to altered host immune response including interferon-signaling[13,14] (p=1.25E-4).

FXR, VSG and body composition

Because we and others have consistently observed increased circulating total bile acids[9,10,15,16] and increased FXR signaling[9,17] following various bariatric procedures including VSG, and because FXR was one of the regulated genes identified in our pathway analysis, we hypothesized that FXR-signaling contributes to the metabolic benefits of VSG. To test this, we first generated whole-body FXR knockout mice (KO), and their wild-type littermate controls (WT) from founders purchased from Jackson Labs (Bar Harbor ME). Because KO mice are somewhat resistant to diet-induced obesity[18] we maintained these mice on a 60% high-fat diet (HFD) for 10 weeks prior to surgery, such that both WT and KO mice became obese. Both genotypes carried more than 30% of their body weight as fat prior to surgery (Fig 2 A-B); our previous data indicate this level of adiposity provides more-than-sufficient opportunity for VSG-induced body weight and fat loss[3,19].

VSG or sham surgery was performed in these obese male WT and KO mice. In the first week after surgery, WT and KO mice lose a comparable amount of weight relative to their sham-operated controls. However, whereas WT-VSG mice maintained this relative weight loss for the duration of the experiment (Fig 2C, RM ANOVA with Tukey posthoc, $p < 0.001$), the KO-VSG animals recovered it. Within 5-weeks, the body weight of KO-VSG

animals was no longer different than sham-operated controls (Fig 2D, RM ANOVA with Tukey posthoc, $p< 0.001$). Moreover, when we measured body composition at post-op week 11, WT-VSG mice had half the body fat of sham-operated WT controls, while the body fat of KO-VSG and KO-sham operated mice was equivalent (Fig 2E-F, 2-way ANOVA with Tukey posthoc, $p< 0.01$).

Notably, KO-sham mice continue to gain weight at a slower rate compared to WT-sham mice following surgery. This represents a caveat to the interpretation of our findings that requires careful consideration. However, the failure of FXR-VSG mice to sustain body weight and body fat loss is unlikely to be a product of KO mice being relatively resistant to diet-induced obesity for two reasons. First, we have observed potent reductions in body fat after VSG in mice that have as little as an average 7g of body fat[3,19], whereas the FXR KO mice in this study had an average of 9g. Second, we executed post-hoc analyses, selecting the heaviest KO and the lightest WT mice to create a subset with comparable body weights and composition prior to the surgery. Importantly, in this subset WT-VSG mice maintain an 11.3g decrement in body weight and 10.2g decrement in body fat compared to WT-SHAM, whereas KO-VSG mice recover to match the body weight and body fat of KO-sham controls within 4-5 weeks. Further, KO-VSG mice are significantly heavier than WT-VSG mice by 8 weeks after surgery (Extended Data Fig 1A-C, 2-way ANOVA with Tukey posthoc, $p< 0.001$) and maintain a greater fat mass than WT-VSG mice at 11 weeks after surgery (Extended Data, Fig 1D,E, 2-way ANOVA with Tukey posthoc, $p< 0.05$).

FXR, VSG and feeding behavior

To understand how KO-VSG animals were able to recover this body weight, we measured weekly HFD intake in these singly-housed mice. Both WT and KO mice consumed fewer calories during the first week following VSG as compared to sham surgery. However, whereas WT-VSG mice maintained this lower food intake for up to 3 weeks (Fig 3A, RM ANOVA with Tukey posthoc, $p< 0.001$), KO-VSG mice were only hypophagic during the first week (Fig 3C, RM ANOVA with Tukey posthoc, $p< 0.001$). Importantly, and in contrast to what occurs when animals are calorically-restricted in the absence of surgery[20], this caloric deficit was not recovered at later time points in WT-VSG mice, allowing for the maintenance of reduced body weight and body fat over the course of the study (Fig 3A,B). On the other hand, beginning in post-op week 4, KO-VSG mice actually consumed *more* food than sham operated controls (Fig 3C,D, Tukey posthoc $p< 0.05$), suggesting that FXR signaling is necessary for the repression of rebound hyperphagia following caloric restriction initially achieved by VSG. This result is also consistent with our growing understanding that VSG is a metabolic, rather than purely restrictive, procedure[6], as both genotypes are left with a similarly small stomach after VSG.

Eight weeks post-surgery, WT-VSG mice had consumed 15% fewer calories than WT-sham mice, but cumulative food intake by KO-VSG mice was equivalent to sham-operated controls (Fig 3E, 2-way ANOVA with Tukey posthoc, $p< 0.01$). Further, when we allowed the mice to choose among three pure macronutrient diets, WT-VSG mice had a significantly reduced preference compared to WT-sham. Unexpectedly, KO-sham mice already exhibit a substantial reduction in the preference for fat compared to WT-sham. This was not further

reduced by VSG (Fig 3F-G, 2-way ANOVA with Tukey posthoc, $p < 0.05$). However, we cannot exclude that the lack of an effect in the KO mice represents a physiological "floor" that cannot be further reduced by VSG.

FXR, VSG and glucose tolerance

To investigate whether FXR-signaling contributes to improvements in glucose tolerance observed following VSG, we challenged fasted mice with an intraperitoneal (i.p.) injection of 1 g/kg·bw dextrose. VSG was associated with a 20% decrease in fasting blood glucose in WT mice, whereas it was associated with a 24% increase in fasting blood glucose in KO mice (Fig 4A, 2-way ANOVA with Tukey posthoc, $p < 0.001$). WT-VSG mice exhibited a substantial improvement in the ability to clear the i.p. injection of glucose, reflected as a 35% reduction in the AUC relative to sham-operated controls. In contrast, KO-VSG and sham-operated mice exhibited no differences in glucose tolerance (Fig. 4B-C, 2-way ANOVA with Tukey posthoc, $p < 0.01$; t-test, $p < 0.001$). While the present findings do not address whether the improvements observed in WT-VSG relative to WT-sham mice are independent of weight loss, we note that KO-VSG and WT-VSG mice were equivalent body weights at the time of this GTT. Despite this, when the glucose excursion of WT-VSG and KO-VSG mice are compared directly, KO-VSG mice exhibit significantly impaired glucose clearance at both 30 and 60 minutes (2-way RM ANOVA with Tukey posthoc, Extended Data Fig2).

FXR, VSG and gut microbial communities

Gut microbial communities are altered in obese individuals[21] and respond to changes in caloric intake and macronutrient content of the diet[22]. Recent evidence implicates dramatic changes in gut microbial communities both in humans and mice, as potential contributors to the benefits of weight-loss surgery[23–26]. Transplantation of the gut microbiota from obese mice into gnotobiotic mice is associated with weight gain[27,28], whereas transplantation of gut microbiota from RYGB mice is associated with reduced weight gain compared to transplantation with sham microbiota[26].

Because bariatric surgery affects the prevalence of many microbial species, it has been difficult to ascertain which specific changes might functionally contribute to its benefits. The present study provides an opportunity to address this question, by comparing the interacting effects of FXR deficiency and VSG on gut microbial ecology. Specifically, because FXR KO mice are refractory to the metabolic benefits of VSG, we infer that any changes in gut microbial communities that occur after VSG irrespective of genotype are not sufficient (but may nonetheless be necessary) to recapitulate its benefits. On the other hand, changes that result from an interaction between genotype and surgery are more likely to be critical to the potent effect of VSG. Pertinent to this, bile acids can modulate the abundance and composition of gut microbes, both directly, and indirectly by activation of FXR-signaling[29,30]. Conversely, the gut microbiota can modify bile acid composition by microbial enzymatic activities, thereby altering both bile acid homeostasis and FXR signaling[31,32].

At sacrifice, 14-weeks following surgery, we extracted genomic DNA from cecal contents and performed pyrosequencing of the 16S rRNA gene. Because all of the mice in this study were maintained on the same purified HFD, and because the average caloric intake by WT-VSG mice was only reduced in the first 3 weeks of this 14-week study (Fig 3), any observed differences are unlikely to be secondary to differing caloric intake or macronutrient content of the diet. Moreover, because WT-VSG, KO-sham, and KO-VSG mice had equivalent body weights at sacrifice, any observed differences among these groups are unlikely to be secondary to differing body weight or composition.

Weighted UniFrac analysis (sensitive to abundances of taxa)[33] showed separation of WT-VSG samples from WT-sham samples along the first component, indicating that VSG had a stronger effect on microbiota composition in WT mice than in KO mice (Fig 5A, Extended Data Fig3, Two-way ANOVA with Tukey posthoc). As shown in Fig 5B-C, the separation of samples in the PCoA plot reflects differences in the Bacteroidetes and Firmicutes levels. In light of these differences we further identified specific taxonomic changes that result from an interaction between genotype and surgery, as these may represent microbial groups that are critical to the potent effects of bariatric surgery—though future studies involving colonization of germ-free mice would be required for definitive evidence supporting a functional involvement.

The relative abundance of several bacteria previously identified as important modulators of systemic metabolism, was altered differently by VSG according to genotype. Specifically, the relative abundance of *Bacteroides* was substantially reduced in WT-VSG mice relative to WT-sham controls, but did not vary with surgery among KO mice (Fig 5D, 2-way ANOVA with Tukey posthoc, $p< 0.05$). A recent study investigating the therapeutic potential of probiotic treatment in obese women found that decreasing prevalence of *Bacteroides* was associated with decreasing adiposity and improved glucose control[34]. Likewise, in the present study, decreasing abundance of *Bacteroides* was associated with decreased weight gain, fat gain (Extended Data Fig4), and decreased AUC in a glucose tolerance test— suggesting a functional association that depends on FXR.

An uncharacterized genus in the Porphyromonadaceae family, a bacterial group negatively correlated with Type-1 diabetes[35], and decreased in HFD-fed mice[22], was substantially increased in WT-VSG mice relative to WT-sham controls. In contrast, this group was reduced in KO-VSG mice relative to their sham-operated controls (Fig 5E, 2-way ANOVA with Tukey posthoc, $p< 0.05$).

Finally, the relative abundance of *Roseburia* was 12-fold higher in WT-VSG ceca compared to WT-sham, but the abundance of this microbe in both KO groups resembled the WT-sham group (Fig 5F, 2-way ANOVA with Tukey posthoc, $p< 0.05$). Importantly, and consistent with our findings, two recent gut metagenome analyses identified decreased abundance of *Roseburia* as highly discriminant for T2DM, in both a European and a Chinese population[36,37]. Likewise, a study investigating the therapeutic effect of a prebiotic treatment in rodents found that increased abundance of *Roseburia* was associated with weight loss and improved glucose tolerance, independent of food intake[38]. In the present study, the abundance of *Roseburia* was negatively correlated with AUC in the glucose

tolerance test (Extended Data Fig4), and this was due primarily to the relationship within the WT-VSG group ($R^2 = 0.75$, $p < 0.05$, Fig 5G), suggesting an FXR-dependent functional association.

In addition we observed genotype-independent changes in the relative abundance of the genera *Lactobacillus* and *Lactococcus* and of Enterobacteriaceae (Extended Data Fig5). Consistent with this, an increase in *E. coli* and other enterobacteria has likewise been reported after RYGB[23,24,26]. Such changes may indeed contribute to the benefits of VSG and other bariatric procedures, but the present data suggest they are not sufficient to elicit improvements in energy balance and glucose homeostasis.

Changes in gut microbiota may influence host metabolism in part due to the ability of the microbiota to attain colonic dietary conversion, resulting mostly in the production of fatty acid end products. Pertinent to this, a wide range of data now links the production of SCFA to various metabolic outcomes[36,37,39,40]. To this end, we measured cecal short-chain fatty acids (SCFAs) and other organic acids produced by the gut microbiota. There were no differences in the total abundance of SCFA among the 4 groups (Extended Data Table1). The relative abundances of butyrate and propionate (Extended Data Fig6A-B), but not acetate (Extended Data Fig6C) were altered by VSG and this did not differ depending on genotype (2-way ANOVA with Tukey posthoc, $p < 0.05$). The resulting decrease in the acetate:butyrate ratio (Extended Data Fig6D, 2-way ANOVA with Tukey posthoc, $p < 0.001$) possibly indicates that acetate is more efficiently converted to butyrate following VSG. Consistent with the increase in *Lactobacillus* and *Lactococcus*, we also observed an increase in lactate following VSG (Extended Data Table1). Again, although such changes may indeed contribute to the benefits of VSG and other bariatric procedures, the present data suggest they are not sufficient to elicit metabolic improvements.

DISCUSSION

Though a number of local physiological and environmental variables may be altered by VSG, here we have identified a critical role for altered bile acid signaling. Taken together, these results demonstrate that a functional FXR pathway is necessary for sustained weight loss, suppression of rebound hyperphagia, and improved glucose control following VSG. Importantly, KO mice have an equivalently small stomach, yet they do not demonstrate the same improvements as WT mice. Thus these findings directly contradict the common assumption that mechanical restriction, resulting from the reduced stomach size, is sufficient to mediate the therapeutic effects of VSG.

In agreement with this, FXR-signaling is implicated in the regulation of lipid and glucose metabolism[41–44]. Initial reports emphasized a protective role, concluding that FXR signaling is necessary for normal glucose homeostasis. FXR KO mice exhibit impaired glucose and insulin tolerance when maintained on a chow diet[41,42], despite modestly elevated plasma bile acids. In apparent contrast, however, they are resistant to HFD-induced obesity and glucose intolerance[18]. Intriguingly, two studies investigating the effect of the synthetic FXR agonist GW4064 on the development of HFD-induced obesity and glucose intolerance[45,46] yielded opposite results. Whereas Watanabe et al. report greater sensitivity to diet-induced

metabolic dysfunction, Ma et al. report resistance to DIO following treatment with GW4064. A major difference between the two studies was route of administration. Watanabe et al. delivered the drug orally via the diet, whereas Ma et al. delivered it intraperitoneally. FXR is expressed in multiple organs important for the regulation of metabolism, including liver, adipose tissue and intestine, and its activation in these compartments may elicit opposing effects on metabolism, perhaps contributing to this discrepancy. Relevant to this, bile acids may also affect metabolism by signaling via the G-protein coupled receptor TGR5, raising the possibility of cross-talk between these systems[47]. Finally, we note these contradictory phenotypes have likewise been observed in the complex regulation of gene expression by other members of the nuclear receptor family. The PPARγ haploinsufficient mouse, for example, is *more* insulin sensitive despite that PPARγ agonists are well-known for their insulin-sensitizing effects[48]. Like PPARγ, FXR and other nuclear receptors may either activate or repress the transcription of target genes, depending on the presence of co-activator and co-repressor complexes. Therefore, loss-of-FXR function might paradoxically be associated with a relative increased expression in a subset of FXR-regulated genes, while still making the animal resistant to treatments that activate FXR. This may explain the present conundrum that FXR KO mice are simultaneously resistant to some of the deleterious metabolic effects of consuming a HFD and also relatively unresponsive to the metabolic benefits of VSG.

Bariatric surgical procedures, such as VSG, are currently the most effective therapy for the treatment of obesity and are moreover associated with substantial improvements in co-morbidities, including T2DM. The underlying molecular mechanisms contributing to these benefits remain largely undetermined, despite offering tremendous potential to reveal new targets for therapeutic intervention. Progress towards this goal has likely been hindered by a widespread belief that surgery exerts its effects simply by making it physically difficult to consume or absorb calories. The current work provides an alternate framework. That is, it identifies FXR-signaling as a molecular mechanism necessary for both key changes to gut microbial communities and many associated metabolic benefits of VSG. Together these findings provide a new understanding of the mechanisms that underlie the benefits of bariatric surgery and suggest new targets for developing less-invasive therapeutic interventions.

Methods

The Institutional Animal Care and Use Committees at the University of Cincinnati and Cincinnati Children's Hospital Medical Center approved all animal protocols.

RNA Seq and unbiased pathway analysis

For RNA-seq followed by unbiased pathway analysis, the distal 1.5 cm of small intestine was collected from 5 VSG and 5 sham-operated, pair-fed male (SPF) C57Bl/6J mice (Jackson Labs, BarHarbour, ME) that were the subjects of a previously-published study[9]. See [ref 9] for further methodological detail. RNA-seq libraries prepared with the Illumina TruSeq RNA preparation kit were sequencing on the Illumina Hi-Seq 2000, with single-end 50bp reads. Analysis was performed in GeneSpring NGS (Agilent Technologies, Santa

Clara, CA), where sequences were aligned to the mm9 reference mouse genome and assigned Ensembl annotations. Aligned gene reads that passed quality controls (quality threshold >=30, zero N's allowed, no multiply mapping reads) were quantified and used to calculated reads per kilobase per million (RPKM). Raw data was normalized using the DeSeq algorithm where reads were thresholded to a minimum read count of 1. An additional filter required at least 10 reads per entity in each sample of either VSG or SPF samples (N=14591 entities). Differentially expressed genes with a fold change of >= 1.5 between VSG and SPF animals (N=882) were submitted to pathway analysis, which assessed significance of overlap between the 882 differential genes and those genes in pathways curated by Wikipathways, BioCyc, BioPax, and Legacy, with a p-value cutoff of 0.05. Raw and normalized data are accessible through NCBI's Gene Expression Omnibus, accession GSE53782.

Surgery

VSG surgery was performed in DIO mice using isofluorane anesthesia. The lateral 80% of the stomach was excised leaving a tubular gastric remnant in continuity with the esophagus superiorly and the pylorus and duodenum inferiorly. The sham procedure involved analogous isolation of the stomach followed by manually applying pressure with blunt forceps along a vertical line between the esophageal sphincter and the pylorus. Mice consumed liquid diet (Osmolite OneCal) for the first 3 post-operative days, and were re-introduced to HFD on day 3.

Mice

10-12 week old male FXR KO mice and their WT littermates, described elsewhere[49] and bred from founders acquired from the Jackson Labs (Bar Harbour, ME), were singly housed in an AAALAC-approved facility with a 12-12 light-dark cycle, and allowed *ad libitum* access to HFD (D12492, Research Diets, New Brunswick, NJ) and water unless otherwise noted. After 10 weeks of HF-feeding, male mice were randomly divided into body weight and fat-matched groups within genotype, and we performed VSG or sham surgery as above. Based on our power analyses, completed using previous data to determine the expected variance and effect sizes, and based on our historical data regarding post-operative mortality, we performed sham surgery on 13 WT and 9 KO mice and VSG surgery on 14 WT and 15 KO mice. 5 KO-VSG and 4 WT-VSG mice died from complications of surgery and were not included in any of the analyses. Food intake and body weight was monitored weekly. Body composition was measured 1 week prior to and 11 weeks following surgery by magnetic resonance imaging (Echo Medical Systems, Houston, TX). An additional 1 WT-sham, 2 KO-VSG and 2 WT-VSG mice died (or were found moribund) during the period of metabolic phenotyping that occurred between weeks 8 and 15. For any given analysis, only mice that are represented throughout the entire timecourse were included. In addition, for the macronutrient preference study, data from several individuals were excluded based on pre-established criteria—in this case, that the mice consistently spilled the powdered macronutrient diets on the cage floor making accurate measurement of what was ingested impossible. For the microbiota analyses, one WT-VSG individual was excluded due to a noted investigator error while collecting the cecal samples at sacrifice.

Investigators conducting the gene expression and microbiota analyses were blind to the experimental groups.

Macronutrient preference

Food choice was assayed during postoperative week 10 using a macronutrient selection paradigm, in which 3 pure macronutrient diets (Harlan Teklad; TD.02521 [carbohydrate], TD.02522 [fat], and TD02523 [protein]) were presented simultaneously in separate containers for 6 days (n= 12 WT-sham, 6 WT-VSG, 8 KO-sham, 7 KO-VSG).

Glucose tolerance tests

Glucose tolerance was assayed during postoperative week 8 in 5-h fasted mice. Blood glucose was measured with AccuCheck meters and strips (Roche, Indianapolis, IN) from the tip of the tail vein in unrestrained animals at baseline, and at regular intervals following an i.p. injection of 1 g/kg·bw dextrose (n= 13 WT-sham, 10 WT-VSG, 9 KO-sham, 10 KO-VSG).

Analysis of gut microbial communities

Whereas much of the microbiota is dead in the feces, the cecum is an active bioreactor with high metabolic fermentative capacity. Thus we focused our study on the cecal microbiota. Cecal microbiota composition was analysed by pyrosequencing of the V1-V2 region from the bacterial 16S rRNA gene. PCR amplicons were generated from cecal DNA obtained from WT and FXR KO mice that underwent either VSG or sham operations (n= 12 WT-sham, 7 WT-VSG, 9 KO-sham, 8 KO-VSG). Sequence data were analyzed by using the QIIME software package (version 1.5.0)[50].

Sample processing, extraction of genomic DNA and amplification for 454 pyrosequencing—Aliquots of cecal material were collected and immediately frozen in liquid nitrogen at the termination of experiment 2. These aliquots were stored at −80°C until extracted: approximately half of each aliquot was used for isolation of genomic DNA and the other half was used for extraction of SCFAs and microbial metabolites.

Genomic DNA was isolated from 50-80 mg of cecal content using the repeated bead beating (RBB) method previously described by Salonen et al[51]. The V1-V2 region of the 16 rRNA gene was amplified using the 27F and 338R primers fused with 454 Titanium sequencing adapters. 338R primers contained unique error-correcting 12-base barcodes that allow to tag PCR products from different samples[52]. Each sample was amplified in triplicate in a reaction volume of 25 μL containing 1.5 U of FastStart Taq DNA Polymerase (Roche), 0.2 μM of each primer and 10-20 ng of genomic DNA. PCR was carried out under the following conditions: initial denaturation for 3 min at 95°C, followed by 25 cycles of denaturation for 20 sec at 95°C, annealing for 20 sec at 52°C and elongation for 60 sec at 72°C, and a final elongation step for 8 min at 72°C. Triplicates were combined, purified with the NucleoSpin Gel and PCR Clean-up kit (Macherey-Nagel, Germany) and then quantified using the Quant-iT PicoGreen dsDNA kit (Invitrogen, Carlsbad, CA). Purified PCR products were diluted to a concentration of 20 ng/μl and pooled in equal amounts. The pooled amplicons were purified again with the Ampure magnetic purification beads (Agencourt, Danvers,

MA) to remove short amplification products. Sequencing was performed using 454 GS FLX titanium chemistry at GATC Biotech (Konstanz, Germany).

Analysis of 16S rRNA gene sequences—Raw data were quality filtered to remove sequences that were shorter than 200 nucleotides, longer than 1000 nucleotides, contained primer mismatches, ambiguous bases, uncorrectable barcodes, or homopolymer runs in excess of six bases. Quality filtered reads were trimmed of 454 adapter and barcode sequences, and were analysed with the software package Quantitative Insights Into Microbial Ecology (QIIME)[50] (version 1.5.0). A total of 376965 sequences were obtained for 36 samples; sequences were demultiplexed and an average of 10471 sequences were attributed to each sample (range: 7208-12522 sequences).

Sequences were assigned to operational taxonomic units (OTUs) using UCLUST with a 97% threshold of pairwise identity. The most abundant sequence was picked as representative for each OTU and was given taxonomic assignment using the Ribosomal Database Project (RDP) Classifier[4]. Representative OTUs were aligned using Pynast[53] and used to build a phylogenetic tree with FastTree[54] , which was used to estimate β-diversity of samples (weighted UniFrac[33]). Sequences were checked for chimeras using ChimeraSlayer and chimeric sequences were excluded from all downstream analyses. Similarly, singletons and sequences that could not be aligned with Pynast were also excluded.

Extraction of microbial metabolites (SCFAs and other organic acids)—GC-MS was used for measurement of organic acids in mouse cecal samples (n= 12 WT-sham, 7 WT-VSG, 9 KO-sham, 8 KO-VSG). After extraction with diethyl ether, an aliquot of each sample was derivatized with N-tert-butyldimethylsilyl-N-methyltrifluoracetamide (MTBSTFA; Sigma), and the organic acids were quantified by using a gas chromatograph (Model 7890 A, Agilent Technologies) coupled to a mass spectrometer detector (Model 5975 C, inert XL MSD with triple Axis Detector; Agilent Technologies). 50-80 mg of frozen cecal contents were transferred to glass tubes (16×125 mm) fitted with a screw cap, and a volume of 100 μl of internal standards stock solution ([1-^{13}C]acetate and [$^{2}H_6$]propionate 1 M, [$^{13}C_4$]butyrate 0.5 M, [1-$^{13}C_1$]isobutyrate and [1-^{13}C]isovalerate 0.1 M, [1,2-$^{13}C_2$]hexanoate , [^{13}C]lactate and [$^{13}C_4$]succinic acid each at 40 mM) was added to the tubes . Prior to extraction samples were freeze-dried at −50°C for 3 h (yield 8-15 mg/dry weight). After acidification with 50 μl of 37% HCl, the organic acids were extracted twice in 2 ml of diethyl ether. A 500 μl aliquot of the extracted sample was mixed together with 50 μl of *N*-tert-butyldimethylsilyl-*N*--methyltrifluoracetamide (MTBSTFA; Sigma) at room temperature. An aliquot (1 μl) of the resulting derivatized material was injected into a gas chromatograph (Agilent Technologies 7890 A) coupled to a mass spectrometer detector (Agilent Technologies 5975 C). A linear temperature gradient was used: the initial temperature of 65°C was held for 6 min, increased to 260°C (15°C/min) and then to 280°C for 5 min. The injector and transfer line temperatures were 250°C. Quantitation was completed in selected ion monitoring acquisition mode by comparison to labeled internal standards (valerate was compared to [1-^{13}C]isovalerate, heptanoate and octanoate were compared to [1,2-$^{13}C_2$]hexanoate and fumarate was compared to [$^{13}C_4$]succinic acid). The *m*/*z* ratios of monitored ions were as follows: 117 (acetic acid), 131 (propionic acid), 145

(butyric acid), 146 (isovaleric acid), 159 (isovaleric acid and valeric acid, 173 (hexanoic acid), 187 (heptanoic acid), 201 (octanoic acid), 261 (lactic acid), 287 (fumaric acid), 289 (succinic acid), 121 ([$^{2}H_2$]- and [1-^{13}C]acetate), 136 ([$^{2}H_5$]propionate), 146 ([1-$^{13}C_1$]isobutyrate), 149 ([$^{13}C_4$]butyrate), 160 ([1-^{13}C]isovalerate), 175 ([1,2-$^{13}C_2$]hexanoate), 264 ([^{13}C]lactate) and 293 ([$^{13}C_4$]succinic acid).

Statistical Analyses—Data are presented as mean ± standard errors or as Tukey boxplots, as noted. Data were analyzed using the appropriate ANOVA or repeated measures ANOVA (RM ANOVA), followed by Tukey's posthoc tests, or by t-test as indicated. The data were tested for normality and homogeneity of variance. In cases where the data failed these assumptions, the analyses were also done after rank transformation. In no cases did this alter the statistical significance or interpretation of the findings, so the statistics reported in the figures are from the non-transformed analyses. Data were analyzed using Prism (Graph Pad, San Diego CA) or Sigma Stat (SYSTAT, San Jose CA) software with the critical value, α, set at $p < 0.05$.

ACKOWLEDGEMENTS

We thank Jose Berger, April Haller, Bailing Li, Emily Orr, and Mouhammadoul Toure for expert technical assistance. This work was supported by grants from: UNIK Food Fitness and Pharma for Health and Disease research programme (CC), the Torsten Söderberg and NovoNordisk foundations (FB), Ethicon Endo-Surgery (RK, DAS, RJS), and the NIH (DK082173, HL111319 to KKR, DK093848 to RJS, and the Bioinformatics Core of the Digestive Disease Research Core Center in Cincinnati DK078392).

D.A.S. receives research support from Ethicon Endo-Surgery, Novo Nordisk, and Boehringer-Ingelheim, is a consultant for Givaudan and is on the scientific advisory board for Ethicon Endo-Surgery. R. Kohli receives research support from Ethicon Endo-Surgery. F.B. is a founder of and owns equity in Metabogen AB. R.J.S. has received research support from Ethicon Surgical Care, Novo Nordisk, Ablaris, Roche, Boehringer-Ingelheim and Zealand. He has served as a consultant or paid speaker for Ethicon Surgical Care, Eissai, Forrest and Givaudan. He has a small equity position in Zafgen.

REFERENCES

1. Pories WJ. Bariatric surgery: risks and rewards. J. Clin. Endocrinol. Metab. 2008; 93:S89–96. [PubMed: 18987275]
2. Schauer PR, et al. Bariatric surgery versus intensive medical therapy in obese patients with diabetes. N. Engl. J. Med. 2012; 366:1567–76. [PubMed: 22449319]
3. Wilson-Perez HE, et al. Vertical Sleeve Gastrectomy is Effective in Two Genetic Mouse Models of Glucagon-like Peptide-1 Receptor Deficiency. Diabetes. 2013:2380–2385. doi:10.2337/db12-1498. [PubMed: 23434938]
4. Chambers AP, et al. Weight-Independent Changes in Blood Glucose Homeostasis After Gastric Bypass or Vertical Sleeve Gastrectomy in Rats. Gastroenterology. 2011; 141:950–958. [PubMed: 21699789]
5. Karamanakos SN, Vagenas K, Kalfarentzos F, Alexandrides TK. Weight loss, appetite suppression, and changes in fasting and postprandial ghrelin and peptide-YY levels after Roux-en-Y gastric bypass and sleeve gastrectomy: a prospective, double blind study. Ann Surg. 2008; 247:401–407. [PubMed: 18376181]
6. Stefater MA, Wilson-Pérez HE, Chambers AP, Sandoval DA, Seeley RJ. All bariatric surgeries are not created equal: insights from mechanistic comparisons. Endocr. Rev. 2012; 33:595–622. [PubMed: 22550271]
7. Jackness C, et al. Very Low-Calorie Diet Mimics the Early Beneficial Effect of Roux-en-Y Gastric Bypass on Insulin Sensitivity and β-Cell Function in Type 2 Diabetic Patients. Diabetes. 2013; 62:3027–32. [PubMed: 23610060]

8. Bradley D, et al. Gastric bypass and banding equally improve insulin sensitivity and β cell function. J. Clin. Invest. 2012; 122:4667–74. [PubMed: 23187122]
9. Myronovych A, et al. Vertical sleeve gastrectomy reduces hepatic steatosis while increasing serum bile acids in a weight-loss-independent manner. Obesity (Silver Spring). 2013 doi:10.1002/oby.20548.
10. Patti ME, et al. Serum bile acids are higher in humans with prior gastric bypass: potential contribution to improved glucose and lipid metabolism. Obes. (Silver Spring). 2009; 17:1671–1677.
11. Larsson E, et al. Analysis of gut microbial regulation of host gene expression along the length of the gut and regulation of gut microbial ecology through MyD88. Gut. 2012; 61:1124–31. [PubMed: 22115825]
12. Lhoste EF, et al. The human colonic microflora influences the alterations of xenobiotic-metabolizing enzymes by catechins in male F344 rats. Food Chem. Toxicol. 2003; 41:695–702. [PubMed: 12659723]
13. Brodziak F, Meharg C, Blaut M, Loh G. Differences in mucosal gene expression in the colon of two inbred mouse strains after colonization with commensal gut bacteria. PLoS One. 2013; 8:e72317. [PubMed: 23951309]
14. Vijay-Kumar M, et al. Metabolic syndrome and altered gut microbiota in mice lacking Toll-like receptor 5. Science. 2010; 328:228–31. [PubMed: 20203013]
15. Kohli R, et al. Weight Loss Induced by Roux-en-Y Gastric Bypass But Not Laparoscopic Adjustable Gastric Banding Increases Circulating Bile Acids. J. Clin. Endocrinol. Metab. 2013; 98:E708–12. [PubMed: 23457410]
16. Cummings BP, et al. Vertical sleeve gastrectomy improves glucose and lipid metabolism and delays diabetes onset in UCD-T2DM rats. Endocrinology. 2012; 153:3620–32. [PubMed: 22719048]
17. Gerhard GS, et al. A Role for Fibroblast Growth Factor 19 and Bile Acids in Diabetes Remission After Roux-en-Y Gastric Bypass. Diabetes Care. 2013; 36:1859–1864. [PubMed: 23801799]
18. Prawitt J, et al. Farnesoid X receptor deficiency improves glucose homeostasis in mouse models of obesity. Diabetes. 2011; 60:1861–71. [PubMed: 21593203]
19. Chambers AP, et al. The effects of vertical sleeve gastrectomy in rodents are ghrelin independent. Gastroenterology. 2013; 144:50–52. e5. [PubMed: 22995675]
20. Ryan KK, Woods SC, Seeley RJ. Central nervous system mechanisms linking the consumption of palatable high-fat diets to the defense of greater adiposity. Cell Metab. 2012; 15:137–49. [PubMed: 22244528]
21. Ley RE, et al. Obesity alters gut microbial ecology. Proc. Natl. Acad. Sci. U. S. A. 2005; 102:11070–5. [PubMed: 16033867]
22. Parks BW, et al. Genetic control of obesity and gut microbiota composition in response to high-fat, high-sucrose diet in mice. Cell Metab. 2013; 17:141–52. [PubMed: 23312289]
23. Zhang H, et al. Human gut microbiota in obesity and after gastric bypass. Proc. Natl. Acad. Sci. U. S. A. 2009; 106:2365–70. [PubMed: 19164560]
24. Furet J-P, et al. Differential adaptation of human gut microbiota to bariatric surgery-induced weight loss: links with metabolic and low-grade inflammation markers. Diabetes. 2010; 59:3049–57. [PubMed: 20876719]
25. Graessler J, et al. Metagenomic sequencing of the human gut microbiome before and after bariatric surgery in obese patients with type 2 diabetes: correlation with inflammatory and metabolic parameters. Pharmacogenomics J. 2012 doi:10.1038/tpj.2012.43.
26. Liou AP, et al. Conserved shifts in the gut microbiota due to gastric bypass reduce host weight and adiposity. Sci. Transl. Med. 2013; 5:178ra41.
27. Turnbaugh PJ, et al. An obesity-associated gut microbiome with increased capacity for energy harvest. Nature. 2006; 444:1027–31. [PubMed: 17183312]
28. Turnbaugh PJ, Bäckhed F, Fulton L, Gordon JI. Diet-induced obesity is linked to marked but reversible alterations in the mouse distal gut microbiome. Cell Host Microbe. 2008; 3:213–23. [PubMed: 18407065]

29. Merritt ME, Donaldson JR. Effect of bile salts on the DNA and membrane integrity of enteric bacteria. J. Med. Microbiol. 2009; 58:1533–41. [PubMed: 19762477]
30. Islam KBMS, et al. Bile acid is a host factor that regulates the composition of the cecal microbiota in rats. Gastroenterology. 2011; 141:1773–81. [PubMed: 21839040]
31. Sayin SI, et al. Gut Microbiota Regulates Bile Acid Metabolism by Reducing the Levels of Tauro-beta-muricholic Acid, a Naturally Occurring FXR Antagonist. Cell Metab. 2013; 17:225–35. [PubMed: 23395169]
32. Swann JR, et al. Systemic gut microbial modulation of bile acid metabolism in host tissue compartments. Proc. Natl. Acad. Sci. U. S. A. 2011; 108(Suppl):4523–30. [PubMed: 20837534]
33. Lozupone C, Knight R. UniFrac: a new phylogenetic method for comparing microbial communities. Appl. Environ. Microbiol. 2005; 71:8228–35. [PubMed: 16332807]
34. Dewulf EM, et al. Insight into the prebiotic concept: lessons from an exploratory, double blind intervention study with inulin-type fructans in obese women. Gut. 2012 doi:10.1136/gutjnl-2012-303304.
35. Wen L, et al. Innate immunity and intestinal microbiota in the development of Type 1 diabetes. Nature. 2008; 455:1109–13. [PubMed: 18806780]
36. Qin J, et al. A metagenome-wide association study of gut microbiota in type 2 diabetes. Nature. 2012; 490:55–60. [PubMed: 23023125]
37. Karlsson FH, et al. Gut metagenome in European women with normal, impaired and diabetic glucose control. Nature. 2013; 498:99–103. [PubMed: 23719380]
38. Neyrinck AM, et al. Dietary modulation of clostridial cluster XIVa gut bacteria (Roseburia spp.) by chitin-glucan fiber improves host metabolic alterations induced by high-fat diet in mice. J. Nutr. Biochem. 2012; 23:51–9. [PubMed: 21411304]
39. Ridaura VK, et al. Gut microbiota from twins discordant for obesity modulate metabolism in mice. Science. 2013; 341:1241214. [PubMed: 24009397]
40. Vrieze A, et al. Transfer of intestinal microbiota from lean donors increases insulin sensitivity in individuals with metabolic syndrome. Gastroenterology. 2012; 143:913–6. e7. [PubMed: 22728514]
41. Cariou B, et al. The farnesoid X receptor modulates adiposity and peripheral insulin sensitivity in mice. J. Biol. Chem. 2006; 281:11039–49. [PubMed: 16446356]
42. Ma K, Saha PK, Chan L, Moore DD. Farnesoid X receptor is essential for normal glucose homeostasis. J. Clin. Invest. 2006; 116:1102. [PubMed: 16557297]
43. Zhang Y, et al. Activation of the nuclear receptor FXR improves hyperglycemia and hyperlipidemia in diabetic mice. Proc. Natl. Acad. Sci. U. S. A. 2006; 103:1006–11. [PubMed: 16410358]
44. Porez G, Prawitt J, Gross B, Staels B. Bile acid receptors as targets for the treatment of dyslipidemia and cardiovascular disease. J. Lipid Res. 2012; 53:1723–37. [PubMed: 22550135]
45. Ma Y, Huang Y, Yan L, Gao M, Liu D. Synthetic FXR agonist GW4064 prevents diet-induced hepatic steatosis and insulin resistance. Pharm. Res. 2013; 30:1447–57. [PubMed: 23371517]
46. Watanabe M, et al. Lowering bile acid pool size with a synthetic farnesoid X receptor (FXR) agonist induces obesity and diabetes through reduced energy expenditure. J. Biol. Chem. 2011; 286:26913–20. [PubMed: 21632533]
47. Thomas C, Pellicciari R, Pruzanski M, Auwerx J, Schoonjans K. Targeting bile-acid signalling for metabolic diseases. Nat. Rev. Drug Discov. 2008; 7:678–9. [PubMed: 18670431]
48. Miles PD, Barak Y, He W, Evans RM, Olefsky JM. Improved insulin-sensitivity in mice heterozygous for PPAR-gamma deficiency. J Clin Invest. 2000; 105:287–292. [PubMed: 10675354]
49. Sinal CJ, et al. Targeted disruption of the nuclear receptor FXR/BAR impairs bile acid and lipid homeostasis. Cell. 2000; 102:731–44. [PubMed: 11030617]
50. Caporaso JG, et al. QIIME allows analysis of high-throughput community sequencing data. Nat. Methods. 2010; 7:335–6. [PubMed: 20383131]

51. Salonen A, et al. Comparative analysis of fecal DNA extraction methods with phylogenetic microarray: effective recovery of bacterial and archaeal DNA using mechanical cell lysis. J. Microbiol. Methods. 2010; 81:127–34. [PubMed: 20171997]

52. Hamady M, Walker JJ, Harris JK, Gold NJ, Knight R. Error-correcting barcoded primers for pyrosequencing hundreds of samples in multiplex. Nat. Methods. 2008; 5:235–7. [PubMed: 18264105]

53. Caporaso JG, et al. PyNAST: a flexible tool for aligning sequences to a template alignment. Bioinformatics. 2010; 26:266–7. [PubMed: 19914921]

54. Price MN, Dehal PS, Arkin AP. FastTree: computing large minimum evolution trees with profiles instead of a distance matrix. Mol. Biol. Evol. 2009; 26:1641–50. [PubMed: 19377059]

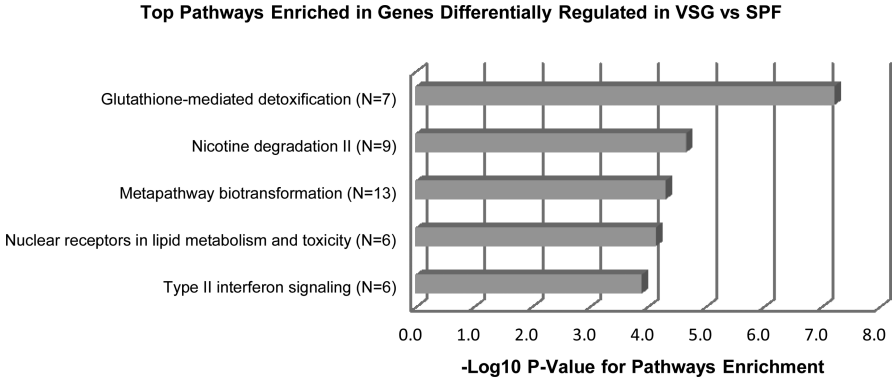

Pathway	VSG vs SPF Genes Represented in Pathway
Glutathione-mediated detoxification (N=7)	Gstm6, Gstm3, Anpep, Gsta4, Gsta1, Gsta2, Gstt1
Nicotine degradation II (N=9)	Aoc1, Fmo1, Ugt2b5, Cyp3a16, Cyp2a41b, Cyp3a41a, Cyp3a11, Inmt, Cyp2b10
Metapathway biotransformation (N=13)	Ugt1a6a, Fmo1, Gstm7, Ugt2a3, Inmt, Cyp26b1, Chst8, Cyp2r1, Gsta4, Gsta1, Gsta2, Gstt1, Chst7
Nuclear receptors in lipid metabolism and toxicity (N=6)	Nr1i3, Abca1, Abcb1a, Abcb4, Cyp2b10, Nr1h4
Type II interferon signaling (N=6)	Gbp1, Cxcl10, Reg1, Nox2, Socs3, Irf4

Figure 1. Unbiased pathway analysis in VSG ileum

Based on a pathway analysis of genes differentially regulated (fold change >=1.5) in the terminal ileum of VSG mice relative to sham-operated, pair-fed (SPF) controls, the following top 5 pathways were significantly enriched: Glutathione mediated detoxification (p=6.00E-8), Nicotine degredation (p=5.64E-4), Metapathway biotransformation (p=4.81E-5), Nuclear receptors in lipid metabolism and toxicity (p=7.18E-5), and Type II interferon signaling (p=1.25E-4). n= 5 per group.

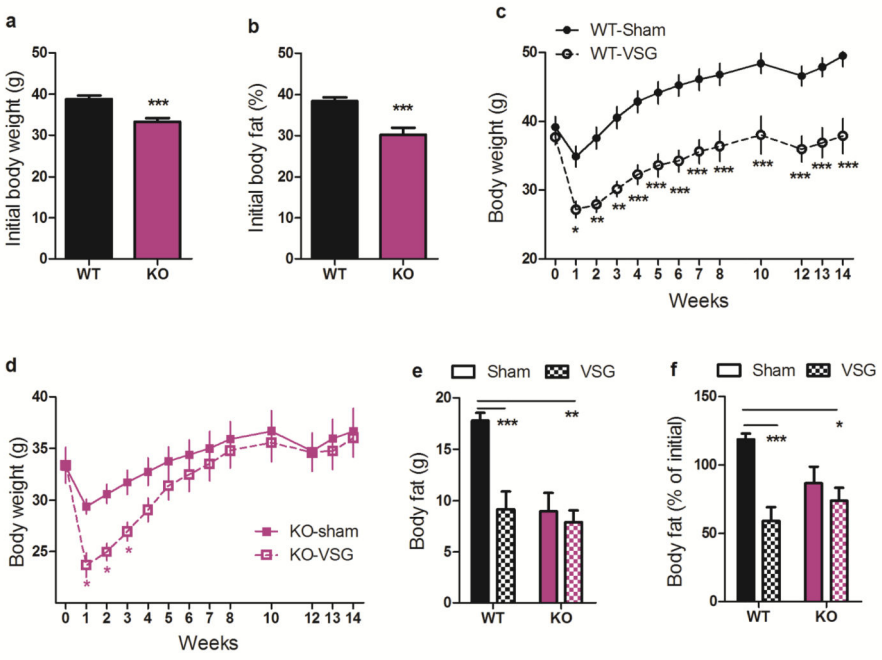

Figure 2. FXR contributes to the maintenance of weight loss following VSG

Both WT and FXR KO mice **A)** weighed more than 30g and **B)** carried more than 30% of their weight as fat prior to the surgery. **C)** WT-VSG mice lose weight and maintain this weight loss, relative to WT-sham controls, whereas **D)** KO-VSG mice recover the initial weight loss within 5 weeks after surgery, relative to KO-sham controls. **E)** 11-weeks following surgery, WT-VSG mice carry half the body fat of WT-sham mice whereas the body fat of KO-VSG and KO-sham mice is equivalent. **F)** 11-weeks following surgery, WT-VSG mice have lost 41% of their pre-surgical body fat, whereas KO-VSG mice exhibit no significant fat loss. Data are shown as mean ± SE. *= p< 0.05, ** = p< 0.01, *** = p< 0.001. For panels A-D, n= 12 WT-sham, 8 WT-VSG, 9 KO-sham, 8 KO-VSG. For panels E-F, n= 12 WT-sham, 9 WT-VSG, 9 KO-sham, 10 KO-VSG.

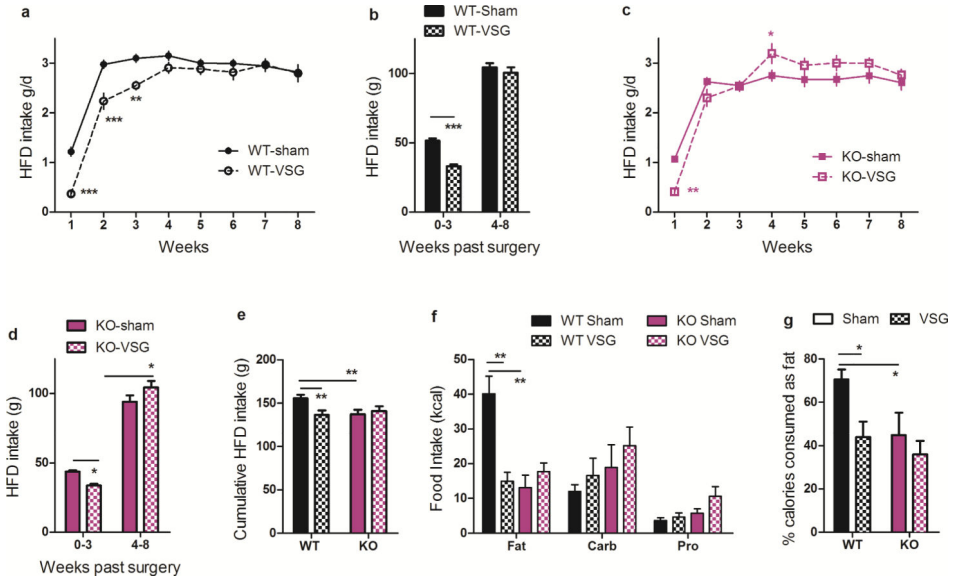

Figure 3. FXR alters feeding behavior following VSG

A,B) WT mice eat significantly less during the first 3 weeks following VSG vs. sham surgery; this is not recovered at later time points. **C,D)** KO mice eat significantly less during the first week following VSG vs. sham surgery; beginning at week 4 KO-VSG mice compensate for this initial caloric deficit by consuming more calories than sham-operated controls. **E)** By 8-weeks following surgery, cumulative food intake by WT-VSG mice was 15% less than WT-sham mice, whereas food intake by KO-VSG and sham-operated mice was equivalent. **F)** When given the choice among three pure macronutrient diets, WT-VSG mice exhibit a blunted preference for dietary fat relative to carbohydrates and protein. **G)** Among WT mice, VSG reduces the preference for dietary fat. Moreover, loss of FXR is associated with lack of preference for dietary fat that is not further altered by the surgery. Data are shown as mean ± SE. * = $p< 0.05$, ** = $p< 0.01$, *** = $p< 0.001$. For panels A-E, n= 13 WT-sham, 10 WT-VSG, 9 KO-sham, 10 KO-VSG. For panels F-G, n= 12 WT-sham, 6 WT-VSG, 8 KO-sham, 7 KO-VSG.

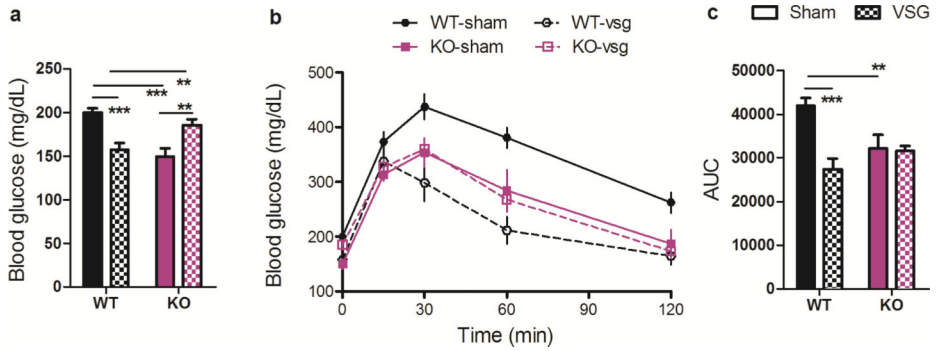

Figure 4. FXR contributes to the improvement in glucose tolerance observed following VSG

A) Among WT mice, fasting blood glucose is reduced following VSG, whereas among KO mice it is increased. **B-C)** Among WT mice, VSG improves the excursion of blood glucose following an i.p. bolus of 1 g/kg dextrose; among KO mice the glucose tolerance of VSG and sham-operated mice is equivalent. Data are shown as mean ± SE. * = p< 0.05, ** = p< 0.01, *** = p< 0.001. n= 13 WT-sham, 10 WT-VSG, 9 KO-sham, 10 KO-VSG.

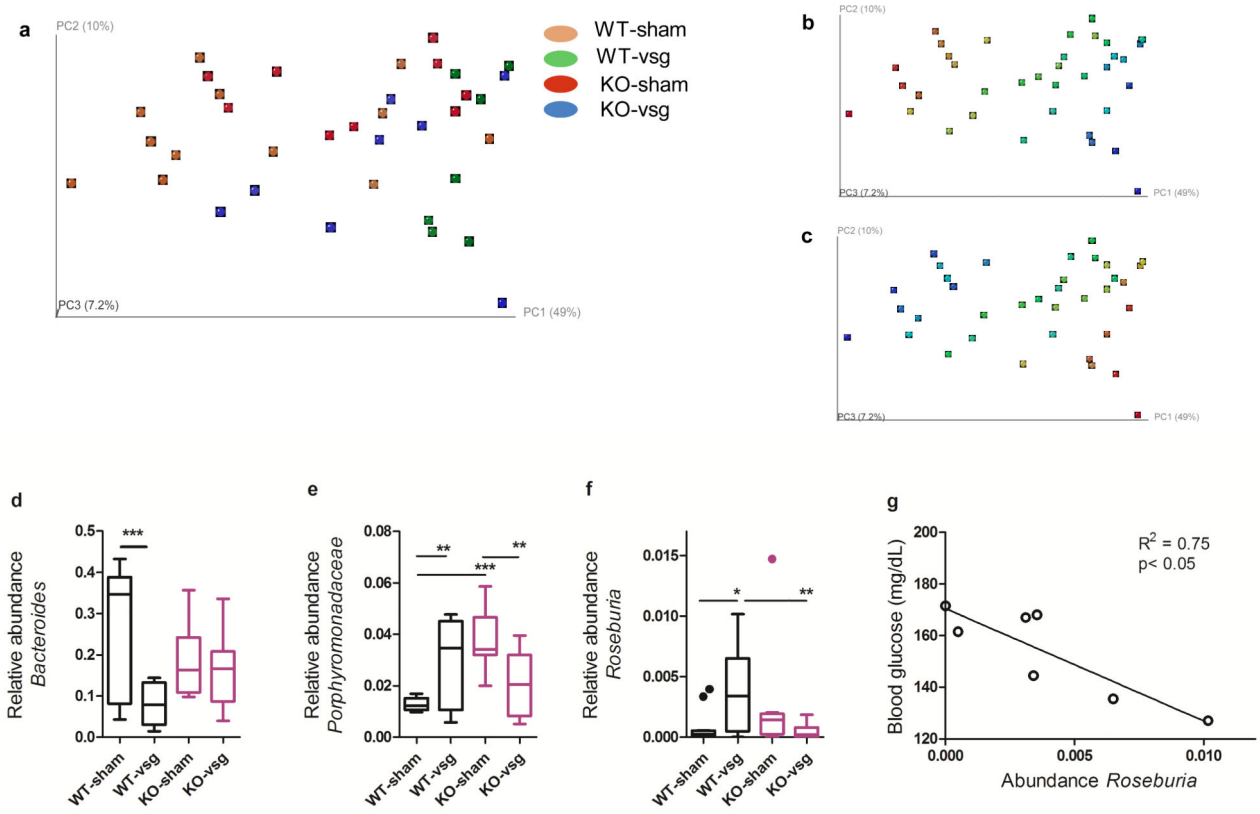

Figure 5. VSG and FXR alter the composition of cecal microbial communities

A) Principal coordinates analysis (PCoA) plot of weighted UniFrac distances. Each dot represents a cecal community. The percentage of variation explained by each principal coordinate is shown in parentheses. **B)** Abundance gradient of Bacteroidetes and **C)** abundance gradient of Firmicutes. Gradients range from blue (indicating low relative abundance) to red (indicating high relative abundance). The same plots are shown for A–C). **D)** Relative abundance of *Bacteroides* was reduced in WT-VSG compared to WT-sham operated mice, but did not differ in KO mice **E)** Relative abundance of one genus in the Porphyromonadaceae family was increased in WT-VSG compared to WT-sham operated mice, but was reduced in KO-VSG mice relative to KO-sham operated controls **F)** Relative abundance of *Roseburia* was increased in WT-VSG compared to WT-sham operated mice, but did not differ in KO mice **G)** Among WT-VSG mice, the relative abundance of *Roseburia* was tightly correlated with fasting blood glucose. Data are presented as Tukey boxplots. * = p< 0.05, ** = p< 0.01, *** = p< 0.001. n= 12 WT-sham, 7 WT-VSG, 9 KO-sham, 8 KO-VSG.

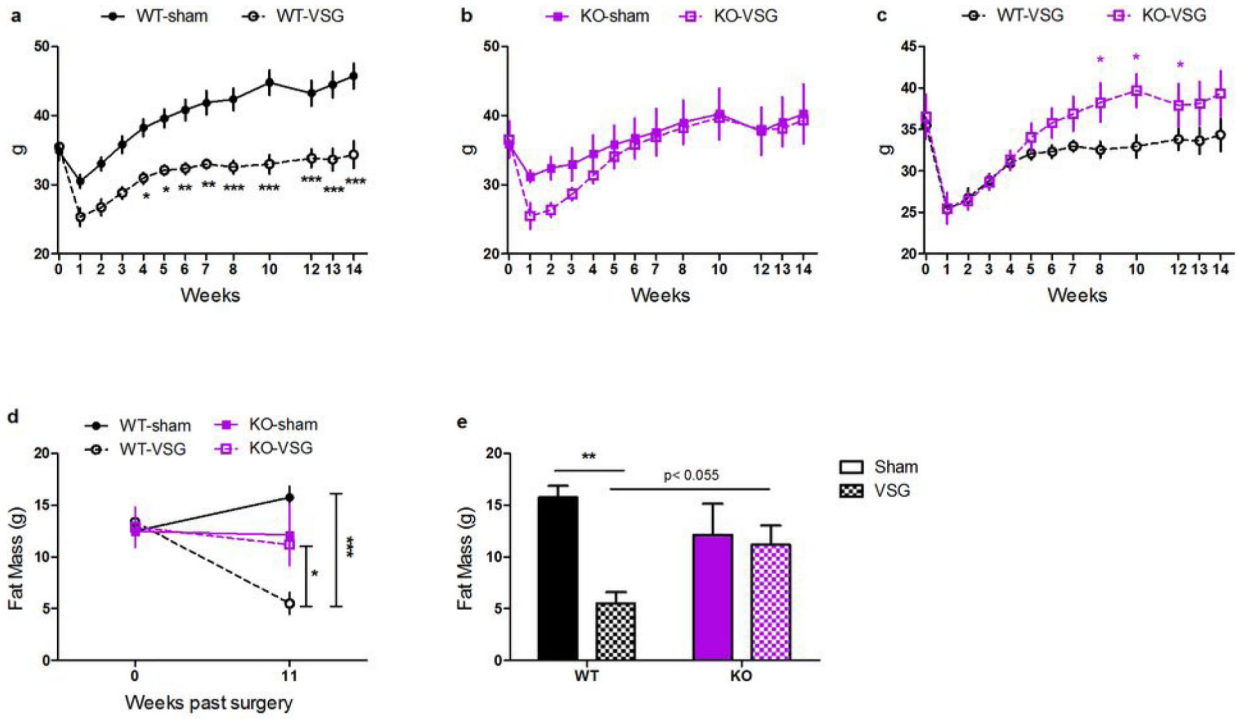

Extended Data Figure 1. Body weight and body fat in a weight-matched subset of WT and FXR KO mice

These posthoc analyses include the lightest 9 WT and heaviest 8 FXR-KO mice prior to surgery, creating 4 well-matched groups. In this subset, **(A)** WT-VSG lose weight relative to WT-sham controls, and maintain this weight loss for 14 weeks, whereas **(B)** KO-VSG mice lose weight initially, but recover to match the weight of KO-sham controls within 4-5 weeks. Likewise **(C-D)** these groups were well-matched for pre-surgical body fat. At 11 weeks after surgery, WT-VSG mice had significantly less body fat compared to both WT-sham controls and KO-VSG mice. KO-sham and KO-VSG mice had equivalent adiposity. Data are shown as mean ± SE. *= p< 0.05, ** = p< 0.01, *** = p< 0.001. n= 5 WT-sham, 4 WT-VSG, 4 KO-sham, 4 KO-VSG.

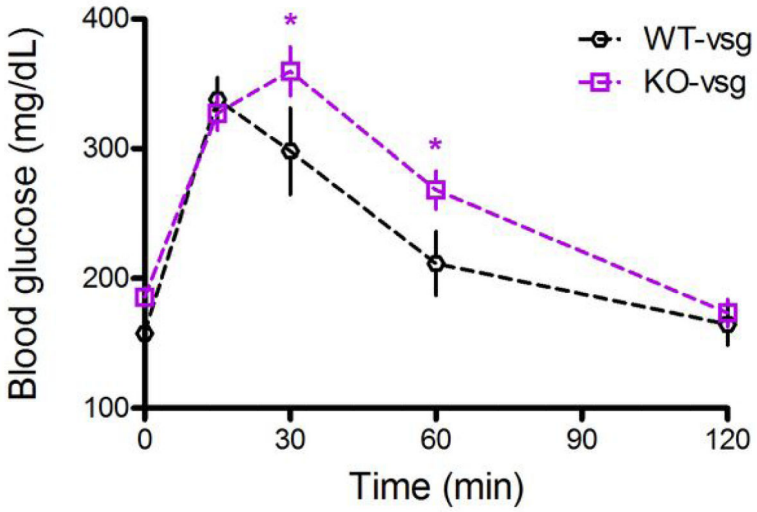

Extended Data Figure 2. Glucose tolerance in FXR-VSG and WT-VSG mice

When the glucose excursion of WT-VSG and KO-VSG mice are compared directly, KO-VSG mice exhibit significantly impaired glucose clearance at both 30 and 60 minutes. Data are shown as mean ± SE. *= $p < 0.05$. n= 10 per group.

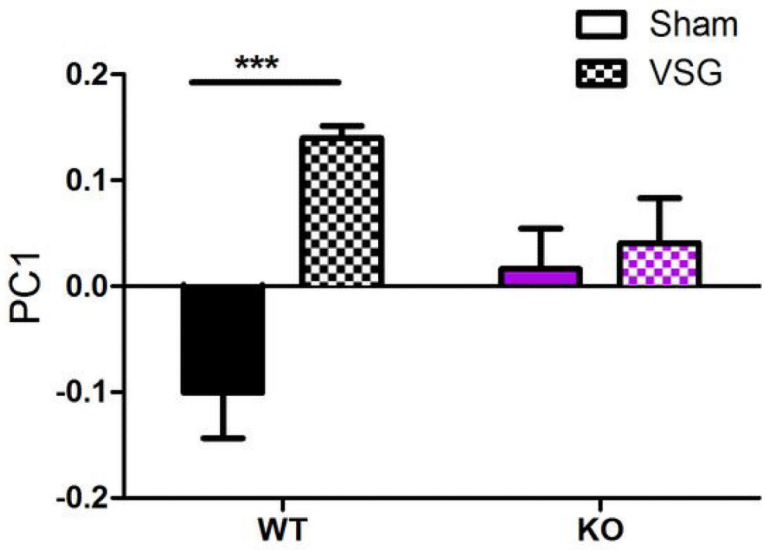

Extended Data Figure 3. Effect of genotype and VSG on distribution along PC1

Among WT mice, sham and VSG mice separate significantly along PC1. In contrast, among KO mice there is no significant difference between sham and VSG. Data are shown as mean ± SE. *= p< 0.05. n= 12 WT-sham, 7 WT-VSG, 9 KO-sham, 8 KO-VSG.

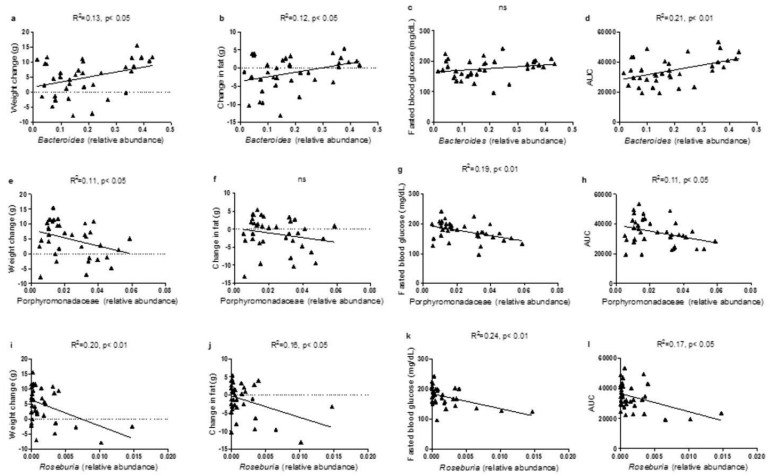

Extended Data Figure 4. Relative abundance of *Bacteroides*, an uncharacterized genus in Porphyromonadaceae, and *Roseburia* correlated with metabolic parameters

The relative abundance of *Bacteroides* was significantly correlated with change in body weight **(A)**, change in body fat **(B)**, and the area under the curve (AUC) in the glucose tolerance test **(D)**, but not with fasting blood glucose **(C).** The relative abundance of an uncharacterized genus in Porphyromonadaceae was significantly correlated with change in body weight **(E)**, fasting blood glucose **(G)**, and the area under the curve (AUC) in the glucose tolerance test **(H)**, but not with change in body fat **(F).** The relative abundance of *Roseburia* was significantly correlated with change in body weight **(I)**, change in body fat **(J)**, fasting blood glucose **(K)**, and the area under the curve (AUC) in the glucose tolerance test **(L).** n=36.

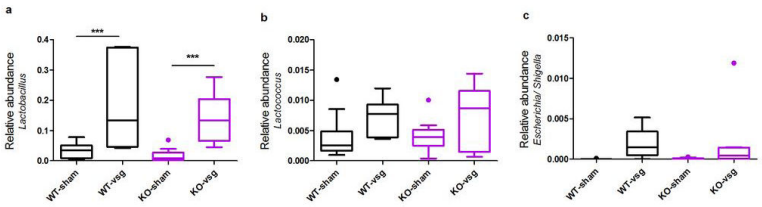

Extended Data Figure 5. Effect of genotype and VSG on the relative abundance of *Lactobacillus, Lactococcus,* and *Escherichia/ Shigella*

VSG was associated with a significant increase in the relative abundance of *Lactobacillus* **(A)**, *Lactococcus* **(B)**, and *Escherichia/ Shigella* that did not vary according to genotype. Data are presented as Tukey boxplots. n= 12 WT-sham, 7 WT-VSG, 9 KO-sham, 8 KO-VSG.

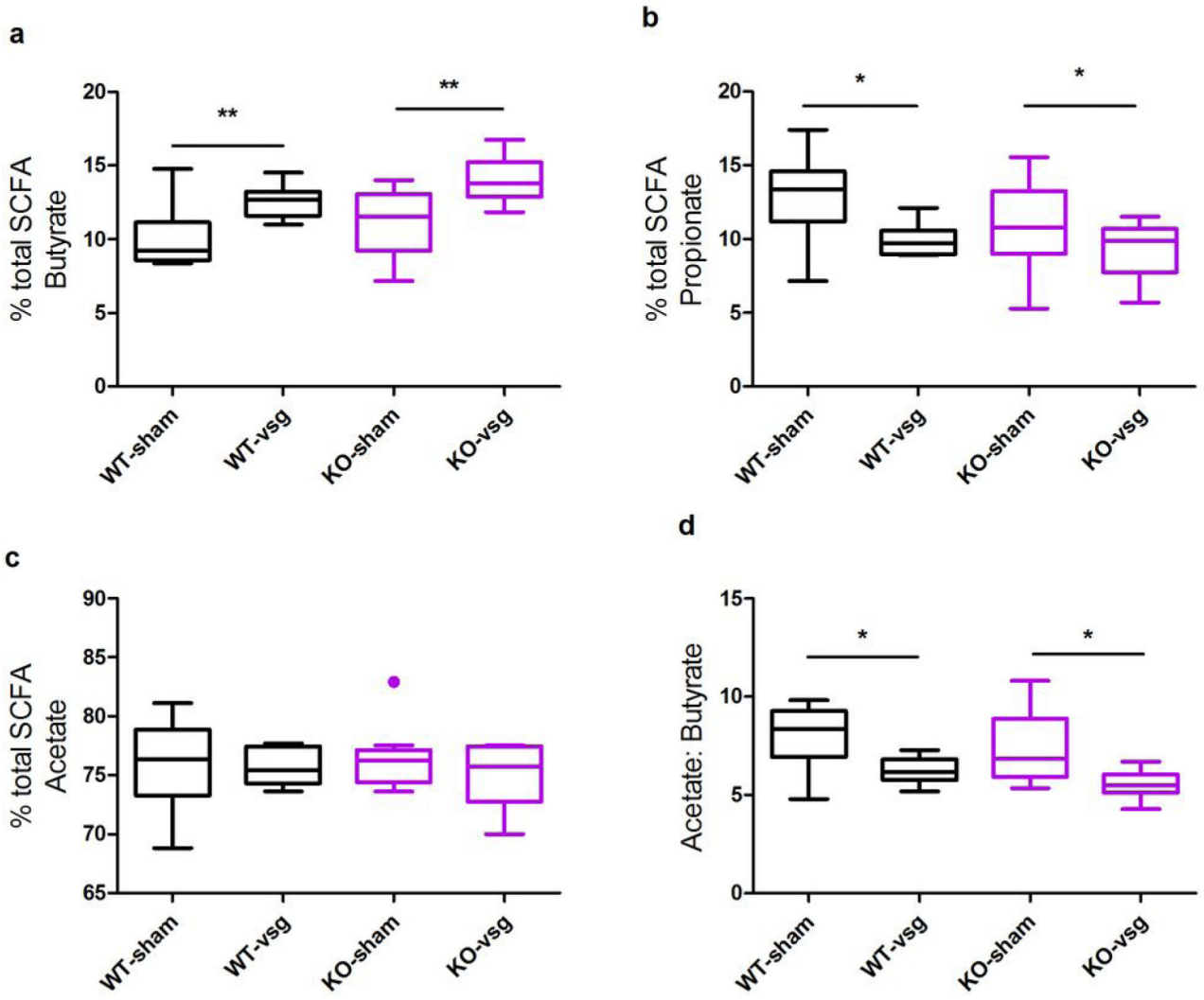

Extended Data Figure 6. VSG alters the abundance of cecal SCFAs

The relative concentration of butyrate **(A)** and propionate **(B)**, but not acetate **(C)** was altered by VSG, and this did not differ depending on genotype. **D)** The acetate:butyrate ratio is increased following VSG. Data are presented as Tukey boxplots. * = p< 0.05, ** = p< 0.01, *** = p< 0.001. Also see Extended Data Table1. n= 12 WT-sham, 7 WT-VSG, 9 KO-sham, 8 KO-VSG.

Organic acid	WT-Sham	WT-VSG	KO-Sham	KO-VSG	p-value (2-way ANOVA)
Acetate (μmol/g)	142.33 ± 20.45	153.46 ± 26.77	124.54 ± 23.61	160.86 ± 25.04	ns
Propionate (μmol/g)	24.80 ± 3.28	19.60 ± 4.29	15.14 ± 3.78	20.32 ± 4.01	ns
Isobutyrate (μmol/g)	9.56 ± 1.71	10.41 ± 2.24	9.11 ± 1.98	10.09 ± 2.09	ns
Butyrate (μmol/g)	19.20 ± 3.42	24.75 ± 4.48	17.55 ± 3.95	29.79 ± 4.19	p (surgery) < 0.05
Isovalerate (μmol/g)	6.25 ± 0.99	7.02 ± 1.3	5.78 ± 1.14	7.08 ± 1.21	ns
Valerate (μmol/g)	2.50 ± 0.41	2.77 ± 0.54	2.19 ± 0.41	2.99 ± 0.41	ns
Hexanoate (μmol/g)	1.14 ± 0.37	1.73 ± 0.49	0.79 ± 0.43	1.74 ± 0.46	ns
Hepthanoate (μmol/g)	0.0080 ± 0.0027	0.0088 ± 0.0027	0.0032 ± 0.0032	0.0088 ± 0.0036	ns
Octanoate (μmol/g)	0.013 ± 0.0056	0.027 ± 0.0073	0.0073 ± 0.0064	0.019 ± 0.0068	ns
Lactate (μmol/g)	13.63 ± 14.80	75.76 ± 19.38	6.95 ± 17.10	38.20 ± 18.13	p (surgery) < 0.01
Succinate (μmol/g)	4.29 ± 2.01	4.55 ± 2.63	5.17 ± 2.32	8.81 ± 2.46	ns
Fumarate (μmol/g)	0.50 ± 0.23	0.82 ± 0.30	0.91 ± 0.27	1.16 ± 0.28	ns
Total SCFAs (C2-C4)	186.33 ± 26.50	197.82 ± 34.70	157.23 ± 30.60	210.99 ± 32.46	ns